Properties and Morphology of Segmented Copoly(ether urea)s with Uniform Hard Segments

Ron M. Versteegen, Ralf Kleppinger, Rint P. Sijbesma,* and E. W. Meijer

Laboratory of Macromolecular and Organic Chemistry, Eindhoven University of Technology, P.O. Box 513, 5600 MB Eindhoven, The Netherlands

Received August 26, 2005; Revised Manuscript Received November 14, 2005

ABSTRACT: Block copoly(ether urea)s with uniform hard blocks consisting of two urea groups possess appealing elastomeric properties. The crystal structure of a model bisurea illustrates the formation of long stacks of hydrogen-bonded urea groups. Thermal analysis of these polymers demonstrates the reversible melting of the hard blocks, causing the material to flow. The low glass transition temperature ensures excellent low-temperature flexibility. The morphology of the material consists of long stacks of associated hard blocks embedded in the soft phase. Elongation of the materials demonstrates their highly elastic behavior, with a strain at break ranging from 1000 to 2100%. During tensile testing, irreversible deformation and reorganization of the hard blocks occur, resulting in a significant amount of tensile set. These well-defined polymers proved to be superior compared to a less-defined analogue having a polydisperse hard block.

1. Introduction

Since the 1940s, many industrial research groups from all over the world have been looking for materials that can be used as an alternative for natural rubber. This led to the discovery of several types of thermoplastic elastomers (TPEs).[1] TPEs possess many of the physical properties of rubbers, i.e., softness, flexibility, and elasticity, but in contrast to conventional rubbers, they can be processed as thermoplastic materials.[2] The cross-links in thermoplastic elastomers are reversible in nature, allowing processing via conventional techniques for thermoplastics, e.g., injection molding and extrusion. The thermoreversible nature of the cross-links in TPEs can be various: e.g., phase separation, crystallization, reversible chemical bonding,[3] hydrogen bonding,[4] metal complexation, or electrostatic interactions.[5] Many TPEs consist of a segmented structure of alternating soft and hard blocks. The hard blocks are generally based on polyester,[1,6] polyamide,[7] or polyurethane[8] segments. At ambient temperatures, the hard blocks are incompatible with the soft blocks. This induces microphase separation by crystallization or liquid−liquid demixing. Cella proposed a morphology of these segmented copolymers in which the hard blocks form crystalline domains.[9] Hard blocks that are not crystallized are dissolved in the amorphous, soft phase, and this incomplete phase separation leads to an increase of the glass transition temperature of the soft phase, which is undesired for the low-temperature flexibility and elasticity of the material. Upon deformation of these materials, irreversible changes in their morphologies may occur. Above the yield point, the hard blocks are disrupted and will reorganize, resulting in energy dissipation and incomplete recovery to their initial dimensions. This hysteresis leads to irreversible changes in the polymer properties, i.e., Young's modulus.

The synthetic procedure to prepare many segmented copolymers has the intrinsic disadvantage that it leads to a distribution in the hard block lengths.[10] This results in a quite inhomogeneous chemical composition of the segmented copolymer. The dispersities in hard and soft block length directly influence the material properties of the polymers. The phase separation within these block copolymers is incomplete.[1] Part of the hard blocks, in particular the shorter ones, are dissolved in the soft phase. The polydispersity of the hard block is manifested in a broad melting range and a rubbery plateau that is dependent on temperature, which is unfavorable.

To improve these properties, and to get more insight into the structure−properties relationship, block copolymers containing hard blocks of uniform length have been prepared.[11,12] The properties of these materials were compared to those of the analogous materials having polydisperse hard blocks, and these studies showed the advantages of the well-defined molecular structure. The materials showed higher crystallinity and better phase separation, causing the properties to be less dependent on temperature. The ultimate properties of the material improved considerably: higher strengths and strains at break were achieved.

Although urea groups are well-known to assemble strongly in a predictable fashion, TPEs possessing hard blocks comprising solely urea groups have only been reported occasionally.[13] In the 1980s Yilgor and co-workers described siloxane-urea containing segmented copolymers, prepared from α,ω-bis-(aminopropyl)poly(dimethylsiloxane) oligomers and various diisocyanates.[13a,b] The mechanical and thermal behavior of these copolymers was studied in detail. Riess et al. recently showed the gelation properties of such segmented siloxane−ureas in silicone fluids such as dimethylcyclosiloxanes.[13f] Bouteiller and co-workers reported the synthesis and mechanical properties of poly(dimethyl)siloxanes to which bisurea moieties were grafted.[13i] Very recently, Yilgor extended this approach to segmented copolymers containing pTHF (PTMO) as the soft block.[13j]

In a previous paper, we described the synthesis and characterization of segmented copoly(ether urea)s, $pTHF_y$-U_x, of which the hard blocks are uniform in length.[14] In this notation, x is the number of urea groups in the hard block, and y is the number-averaged molecular weight of the pTHF soft block.

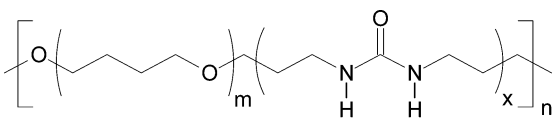

$pTHF_y$-U_x

* Corresponding author. E-mail: R.P.Sijbesma@tue.nl.

10.1021/ma051874e CCC: $33.50 © 2006 American Chemical Society
Published on Web 12/17/2005

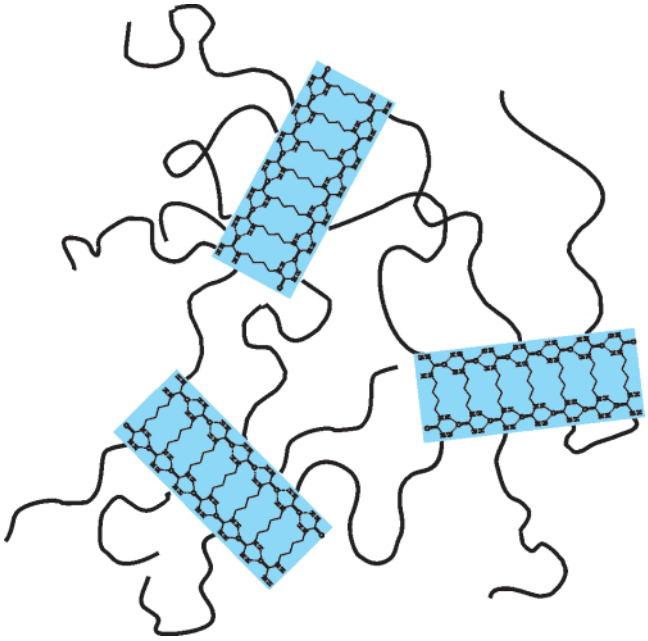

Figure 1. Schematic representation of a block copolymer with a urea hard block.

Table 1. Copoly(ether urea)s with Bis(ureido)butylene Hard Blocks

copolymer	soft block	hard block content (%)
$pTHF_{350}$-U_2	$pTHF_{350}$	33.0
$pTHF_{1100}$-U_2	$pTHF_{1100}$	13.5
$pTHF_{2000}$-U_2	$pTHF_{2000}$	7.9
$pTHF_{2900}$-U_2	$pTHF_{2900}$	5.6
$pTHF_{4000}$-U_2[a]	$pTHF_{4000}$	4.1
$pTHF_{1100}$-U_{2PD}[b]	$pTHF_{1100}$	13.5

[a] Random copolymer of tetrahydrofuran and ethylene oxide. [b] Polydisperse hard block, on average two urea groups.

It was shown that the hard blocks of these segmented copolymers associate by hydrogen bonding between the urea groups if $x > 1$, resulting in the formation of reversible cross-links, as is schematically depicted in Figure 1 for bisurea hard blocks ($x = 2$). These physical cross-links give the material its mechanical strength and elastic behavior, while the soft, amorphous pTHF phase makes the material flexible.[1]

The polymers with three or four urea groups in the hard block were also shown to be elastic materials, but very strong hydrogen bonding between urea groups in the hard block makes these polymers hard to process. It was concluded that the strength of hydrogen bonding in polymers with a hard block comprising two urea groups separated by a butylene spacer leads to an optimal balance between processability and mechanical properties.

In the present paper, the thermal properties of a series of segmented copoly(ether urea)s with bis(ureido)butylene hard blocks (Table 1) is studied using DSC, DMTA, and infrared spectroscopy.

The mode of aggregation proposed in Figure 1 is used as a guideline to further elucidate the morphology of these polymers. In a recent paper, the structural proposal in Figure 1 was supported by the crystal structure of a model compound, bis-(ureido)butylene derivative **1** (Figure 2).[15]

In the crystal lattice of **1**, the well-known urea bifurcated hydrogen-bonding motif[16] with a urea−urea distance of 4.64 Å leads to the formation of an infinite stack of hydrogen bonds, while the distance between to two outer nitrogen atoms N2 and N2′ is only 10.80 Å. The morphological features that this model compound suggests for polymers containing bis(ureido)butylene

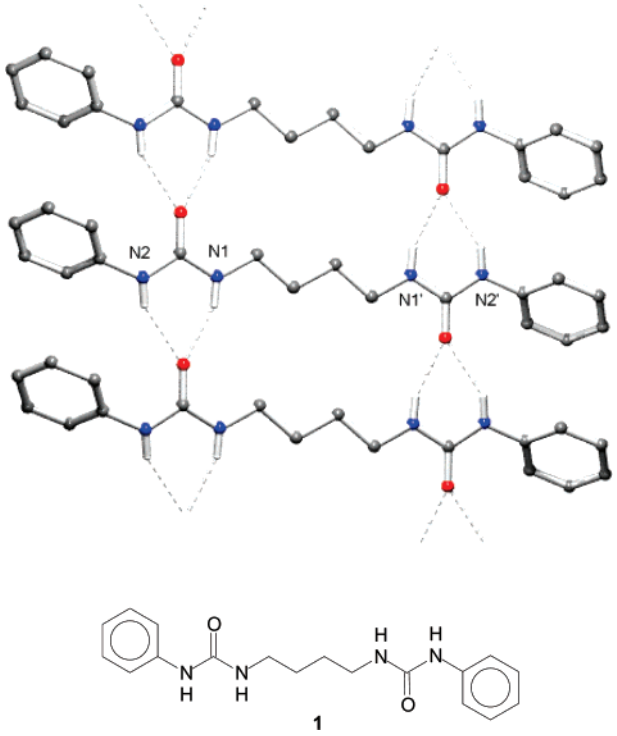

1

Figure 2. Model compound **1** containing a bis(ureido)butylene unit and its mode of aggregation in the crystal.[15]

hard blocks—fibers or lamellae which are very thin,[17] yet extremely long—are investigated using AFM, WAXS, and SAXS. Furthermore, the material properties of this class of thermoplastic elastomers is studied in detail using cyclic tensile testing, while IR and 2-dimensional WAXS are used to investigate strain-induced orientation of the hard blocks of the segmented copolymers.

2. Experimental Section

Temperature-Dependent Infrared Spectroscopy. Infrared spectra were measured on a Perkin-Elmer 1600 FT-IR. Films of the polymer were cast in a potassium bromide pellet and heated in a Linkam THMS 600 heating device.

Differential Scanning Calorimetry. DSC was performed on a Perkin DSC 7; melting and crystallization temperatures were determined at a heating/cooling rate of 10 °C min^{-1} and glass transition temperatures at a heating rate of 40 °C/min.

Dynamic Mechanical Thermal Analysis. DMTA spectra were recorded on a Polymer Laboratories Mk III dynamic mechanical analyzer. A small rectangular bar of the polymer, size approximately 12 × 10 × 0.15 mm, was subjected to a sinusoidal deformation at constant frequency, using the tensile method. Measurements were carried out at a frequency of 1 Hz and a heating rate of 1 °C/min. The amplitude of the sinusoidal deformation was 10 μm, and the static force was 0.2 N in order to ensure good contact between sample and probe.

Atomic Force Microscopy. AFM experiments were performed using a NanoScope III A instrument (Digital Instruments) operating in the tapping mode, utilizing NanoSensor tapping tips. The amplitude of oscillation at free vibration, A_0, was set to 4.0 V. The operating set point ratio (A/A_0) was set to relatively low values ($A/A_0 \sim 0.7$) to obtain best contrast. For visualization of the phase separation in thin copolymer films (typically 1 or 2 μm scan sizes), the phase image gave best contrast.

Small-Angle X-ray Scattering. The small-angle X-ray scattering (SAXS) experiments were performed at the SAXS station of the Dutch-Belgium beamline BM26b of the European Synchrotron radiation facility (ESRF) at Grenoble, using an X-ray wavelength of 0.082 nm and a sample-to-detector distance of about 4 m. Two-

CDV

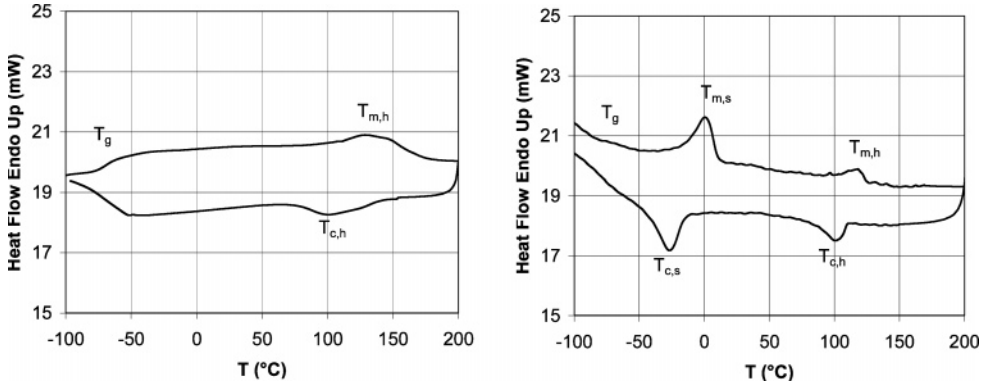

Figure 3. DSC traces of $pTHF_{1100}$-U_2 (left) and $pTHF_{2000}$-U_2 (right) at a heating/cooling rate of 10 °C/min.

dimensional scattering data were recorded with a Gabriel-type multiwire detector having 512 × 512 pixels, each with a size of 300 × 300 μm^2. The detector was placed in an off-center position in order to cover a broad range of scattering vectors from $0.002 < s < 0.04$, where $s = (2/\lambda) \sin \theta$ (with λ the wavelength and 2θ the scattering angle). Individual patterns were normalized with respect to the primary beam intensity and corrected for sample absorption with the aid of ionization chambers placed before and after the sample position.

Two-dimensional scattering pattern from oriented samples were recorded from stacks of the prestrained material in order to obtain an acceptable signal-to-noise ratio. From these patterns a transmission weighted background was subtracted, and the resulting profiles for samples with deformations >150% were analyzed further since in that case a fiber symmetry can be assumed—see $P_2(\lambda)$ parameter from WAXD experiments. In this case, integrations through selected areas in reciprocal space parallel and perpendicular to the orientation axis were performed. The 1D WAXD curves were processed by OTOKO software and deconvoluted by fitting two Gaussian peaks through the data: one amorphous and one crystalline.

Temperature-dependent profiles during heating/cooling cycles were recorded in a temperature range from −25 to 160 °C (rate 5 °C/min), using a remote-controlled LINKAM DSC stage. In this case, linear scattering profiles were extracted by performing a sector integration over the two-dimensional patterns, followed by a subtraction of the transmission-weighted background scattering. The final calibration of the patterns with respect to the scattering vector was based on the diffraction maxima observed for a wet rat-tail collagen ($d \sim 65$ nm).

Initial data processing including normalization to primary beam intensity and detector response as well as background subtraction and sector integrations to obtain linear profiles were performed with DUBBLE software, based on the BSL program. Further evaluations including sections through selected areas of the 2D patterns were performed with the FIT2D software. Processing of the linear profiles including calculation and evaluation of the linear correlation functions was performed with the OTOKO software.

Tensile Testing. Stress−strain measurements were performed on a Zwick Z010 universal tensile tester at an elongation rate of 100%/min. Tensile bars were punched from a solution-cast film of the polymers. Dimensions of the tensile bars: length = 22 mm, width = 5.0 mm, and thickness = 0.30 mm (approximately).

Infrared Linear Dichroism Spectroscopy. Infrared (IR) spectra were recorded by means of a Biorad UMA 500 microscope, coupled to an FTS6000 FT-IR spectrometer. Films of the polymer with a thickness ranging from 10 to 20 μm were cast in a Teflon mold, and tensile bars (22 × 5.0 mm^2) were punched from this. The specimen was elongated and clamped. Infrared spectra were recorded in transmission at 0° and 90° polarization angle with respect to the deformation axis.

3. Results

3.1. Thermal Properties. 3.1.1. Differential Scanning Calorimetry. In first instance, the flow temperatures of the block copoly(ether urea)s were studied by optical microscopy using a Linkam heating device.[14] The temperatures at which the material lost its dimensional stability were determined and are depicted in Table 2. Differential scanning calorimetry (DSC) was used to obtain more quantitative data on the thermal transitions of these materials. The second heating and cooling traces of $pTHF_{1100}$-U_2 and $pTHF_{2000}$-U_2 are depicted in Figure 3; more information is shown in Table 2.

Table 2. Thermal Transitions of Block Copoly(ether urea)s As Determined by DSC[a]

copolymer	T_{flow}[c] (°C)	T_g[d] (°C)	$T_{m,s}$ (°C)	$\Delta H_{m,s}$ (J/g)	$T_{c,s}$ (°C)	$T_{m,h}$ (°C)	$\Delta H_{m,h}$ (J/g)	$T_{c,h}$ (°C)
$pTHF_{350}$-U_2	165	−[b]	−	−	−	158	20.0	145
$pTHF_{1100}$-U_2	140	−68	−	−	−	131	14.2	102
$pTHF_{2000}$-U_2	125	−74	1	20.3	−27	118	3.9	101
$pTHF_{2900}$-U_2	102	−	19	38.3	−10	−	−	−
$pTHF_{4000}$-U_2[e]	100	−73	1	34.9	−37	78	3.6	48
$pTHF_{1100}$-U_{2PD}	135	−69	−	−	−	(1) 114 (2) 142	3.0 0.73	81

[a] Subscripts: s = soft block, h = hard block. [b] Not observed. [c] As determined by optical microscopy.[14] [d] Determined at a heating rate of 40 °C/min. [e] Random copolymer of tetrahydrofuran and ethylene oxide.

For $pTHF_{1100}$-U_2 no melting or crystallization peak for the pTHF-block is observed; it is completely amorphous. Its molecular weight is too low to crystallize, as is often observed in segmented block copolymers possessing pTHF as the soft segments.[1,17,18] The amorphous soft phase shows a glass transition temperature of −68 °C, which is close to the glass transition temperature of pure pTHF,[19] indicating the absence of phase mixing between hard and soft phases. This complete phase separation is advantageous for the low-temperature properties of the material. A broad melting endotherm with a maximum at 131 °C of the hard block is observed. This temperature is close to the flow temperature of 140 °C, which was determined by optical microscopy. Upon cooling, the hard block crystallized at 102 °C.

Increasing the soft block length results in semicrystallinity of the pTHF phase, as is demonstrated in the DSC thermogram of $pTHF_{2000}$-U_2, in which a melting peak at 1 °C and a crystallization peak at −27 °C are observed. Table 2 shows that the crystallinity and melting temperature of the pTHF phase increase with increasing soft block length (series $pTHF_{350}$-U_2 to $pTHF_{2900}$-U_2). Random incorporation of ethylene oxide units in the pTHF chain successfully reduces the crystallinity and melting point of the soft phase, resulting in a completely amorphous soft phase at room temperature. The melting points of the hard blocks correlate well with the flow temperatures, and the same trend is observed of decreasing melting points with increasing soft block lengths. The polymer with the polydisperse hard block shows two melting endotherms, in contrast to the polymers with a uniform hard block.

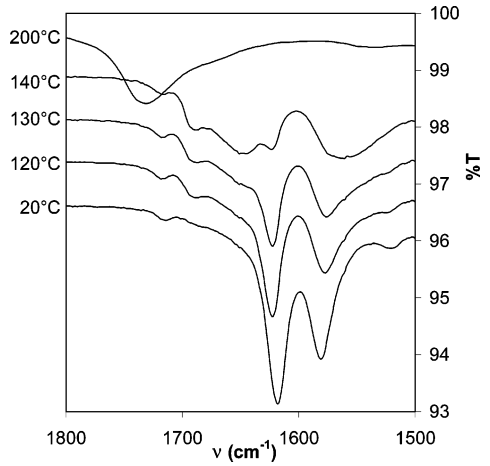

Figure 4. Temperature-dependent infrared spectra of $pTHF_{2000}$-U_2.

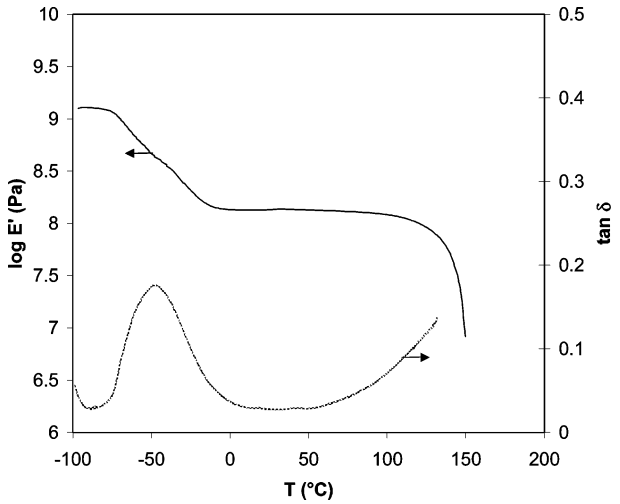

Figure 5. DMTA curves of $pTHF_{1100}$-U_2, measured at 1 Hz and a heating rate of 1 °C/min.

3.1.2. Infrared Spectroscopy. The extent of hydrogen bonding upon heating the material was studied by temperature-dependent infrared spectroscopy. A polymer film was cast from chloroform solution on a potassium bromide pellet, and spectra were recorded in transmission mode. Figure 4 shows the carbonyl region (amide I and amide II vibration) of the infrared spectra at several temperatures of polymer $pTHF_{2000}$-U_2. According to the previously used techniques, the melting temperature of the urea based hard block is between 118 and 125 °C. However, at 130 °C the infrared spectrum still strongly resembled the spectrum at room temperature with a peak corresponding to strong hydrogen bonding ($\nu = 1615$ cm^{-1}). Further heating of the sample resulted in an increase of contributions due to weakly hydrogen bonded ($\nu = 1640$ cm^{-1}) and non-hydrogen-bonded urea groups ($\nu = 1690$ cm^{-1}).[20] Obviously, strong hydrogen bonds between the urea groups are still present in the melt, although the material lost its dimensional stability. Heating the sample to 200 °C for prolonged times resulted in an infrared spectrum in which a new peak at 1730 cm^{-1} dominates. This peak is indicative of degradation of the urea groups,[21] and this process is irreversible. This degradation is also evidenced by discoloration and fuming of the sample.

3.1.3. Dynamic Mechanical Thermal Analysis. Dynamic mechanical thermal analysis (DMTA) was used to study the temperature dependency of the material properties. The storage modulus and tan δ of $pTHF_{1100}$-U_2 are shown in Figure 5. The maximum in tan δ at −50 °C indicates a glass transition, at which the polymer goes from a rigid, glassy material to a rubbery material. From −5 to 110 °C, there is an extended, temperature-independent rubbery plateau ($E' = 135$ MPa). The constant value of this storage modulus is an indication that no phase transitions occur within this temperature range, and phase separation is complete. This is an advantage compared to other thermoplastic elastomers that often show a decrease of the rubbery plateau with increasing temperature, due to incomplete phase separation or partially melting of the hard blocks. Slightly above 120 °C, the hard blocks start to melt, and the material begins to soften. It finally collapses at 148 °C. These temperatures correspond well with those found with DSC and optical microscopy.

Table 3. Characteristics of Block Copoly(ether urea)s As Determined by DMTA

copolymer	T_g (°C)	E'(25 °C) (MPa)	T_{flow} (°C)
$pTHF_{1100}$-U_2	−50	135	148
$pTHF_{2000}$-U_2	n.d.[a]	17	112
$pTHF_{4000}$-U_2	−62	11	105

[a] n.d. = not determined.

In Table 3 some characteristics of other copoly(ether urea)s are depicted. The storage moduli of these materials at 25 °C decrease with increasing soft block length; i.e., the materials become softer with decreasing hard block content.[1,5] The difference in modulus between polymers $pTHF_{1100}$-U_2 and $pTHF_{2000}$-U_2 is remarkably high. Similar to the results found with optical microscopy and DSC, a decrease of flow temperature with increasing soft block length was observed by DMTA.

3.2. Morphology. The morphology of the block copoly(ether urea)s, as proposed by us, is schematically depicted in Figure 1. Long stacks of hydrogen-bonded urea groups, i.e. the hard blocks, are embedded in the amorphous pTHF phase. In this way, reversible cross-links are formed, which give the material its elastomeric properties. To examine the validity of this model, the morphology of $pTHF_{2000}$-U_2 was studied by AFM and X-ray diffraction techniques.

3.2.1. Atomic Force Microscopy. Thin films of ∼30 nm thickness were cast on a silicon wafer from chloroform/methanol solution. These substrates were subsequently heated to 150 °C and slowly cooled to room temperature to allow slow crystallization of the hard blocks. The structures of these films were studied by AFM in the tapping mode. Figure 6 shows the AFM images of polymer $pTHF_{2000}$-U_2, in both height and phase contrast. The resolution of the latter is better. The hard phase appears lighter than the soft phase in this image. Long fibers of the hard block embedded in the soft phase are visible. The length of these fibers ranges to over 500 nm, and the apparent width is estimated at 10 nm. However, smaller details cannot be discerned, since the resolution is limited by the sharpness of the AFM tip. No clear AFM images were obtained from melt-processed films, probably due to the larger thickness of these films.

A very similar hard phase was observed for materials $pTHF_{1100}$-U_2 and $pTHF_{4000}$-U_2.

3.2.2. Wide-Angle X-ray Diffraction. Wide-angle X-ray diffraction (WAXD) and small-angle X-ray scattering (SAXS) have been used extensively to investigate the morphology of thermoplastic elastomeric block copolymers.[1,22,23] Cella proposed the nowadays commonly accepted lamellar morphology for segmented copolymers, in which the crystalline phase consists of hard segments, embedded in a mixed amorphous phase, which consists of the soft segments and uncrystallized hard segments.[9] Bonart has confirmed this domain structure by SAXS.[24]

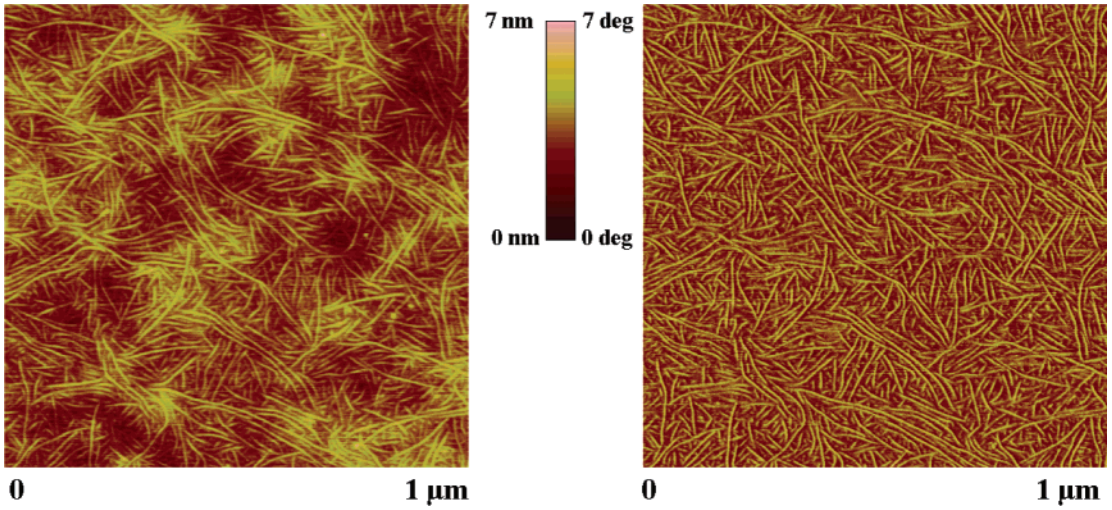

Figure 6. AFM images of $pTHF_{2000}$-U_2; height (left) and phase contrast (right).

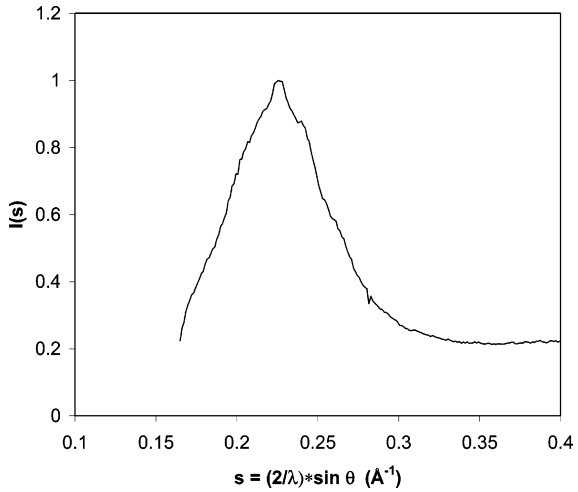

Figure 7. WAXD curve of nonoriented solution-cast sample of $pTHF_{1100}$-U_2.

WAXD and SAXS measurements were carried out on nonoriented solution-cast samples of $pTHF_{1100}$-U_2. Figure 7 shows the WAXD profile of this polymer at room temperature. A broad peak is visible, originating from the amorphous pTHF phase. No reflections are observed that reveal the presence of a crystalline pTHF phase.[25] On top of the broad WAXD peak, a reflection is superimposed at $s = 0.226$ Å^{-1} (d spacing of 4.42 Å). This corresponds well with the spacing between the hydrogen-bonded urea groups (4.6 Å) that was found in the crystal structure of model compound **1** (Figure 2). Because of the low hard block content of this polymer (13.5%), this reflection is rather small.

3.2.3. Small-Angle X-ray Scattering. Figure 8 (top) shows the SAXS curve of the same polymer. The analysis of the small-angle X-ray scattering intensities, $I(s)$, was based on the linear correlation function

$$K_1(r) = \int_0^\infty I(s)s^2 \cos(2\pi rs)\, ds \qquad (1)$$

that was obtained via cosine transformation of the data.[26] It is important to note that this approach is based on a two-phase, lamellar morphology in which the width of the domains is much larger than their thickness. The analysis assumes periodic stacking of crystalline and amorphous domains with a long period, L, and a lamellar thickness of the crystalline domain, d. Despite these assumptions and its limitations, this approach is often used on semicrystalline polymers due to its simplicity and good agreement with results obtained obtained by other techniques.

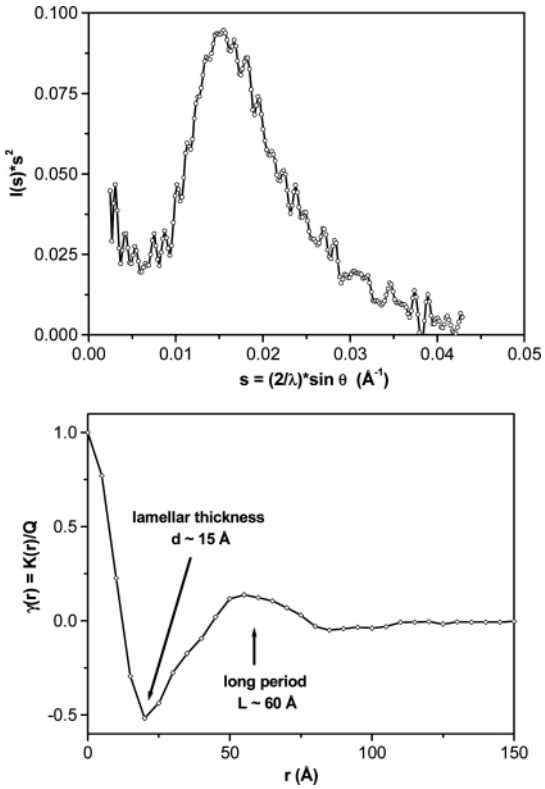

Figure 8. One-dimensional scattering intensities $I_1(s)$ obtained from SAXS experiments on $pTHF_{1100}$-U_2 (top) and the normalized linear correlation function, $\gamma(r)$, calculated from these data (bottom).

The linear correlation function (Figure 8, bottom) reveals the long period, $L = 60$ Å, and the lamellar thickness, $d = 15$ Å. Regardless of the limitations of the applied model, these structural parameters correspond very well to the typical dimensions of the polymer architecture. According to the crystal structure of model compound **1**, the distance between the carbon atoms on the outside of both urea groups is only slightly less than 15 Å (Figure 9).

The lamellar model assumes crystalline domains of infinite size in two dimensions. According to AFM, which shows very long hydrogen-bonded stacks, one dimension can indeed be considered as infinite. However, in the second dimension

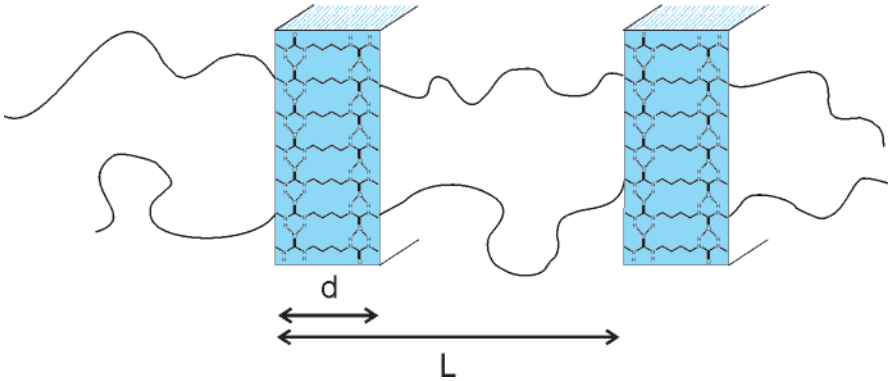

Figure 9. Schematic picture of the morphology of the block copolymer; not all soft blocks are plotted for clarity.

perpendicular to the former one, the size of the crystalline domain cannot be infinite; otherwise, platelike structures would be observed in AFM. Another indication for the limited size is the amount of crystallinity of the sample as estimated from to the SAXS measurements. A long period of 60 Å and a lamellar thickness of 15 Å implies a crystallinity of 25 vol %. However, on the basis of the ratio between hard and soft segments, the crystallinity is expected to be much lower, to be exact 13.5 wt %. This suggests a pseudo-two-phase morphology in which crystalline domains of rather limited size are dispersed in the amorphous matrix.[27] Such a morphology would give rise to a diffuse scattering intensity at very low angles. However, our measurements do not allow for such an analysis due to the limited amount of data points in this region.

3.2.4. Real-Time SAXS/WAXD/DSC Measurements. The melting and order−disorder transition of block copolymers has been studied by temperature-dependent SAXS and/or WAXD experiments.[28] For many thermoplastic elastomers, it is a question whether the crystallization of the hard blocks starts from a homogeneous melt or from a preordered (phase-separated) melt. The latter possibility represents a rather attractive aspect, since crystallization of the hard blocks would use the existing structure as a template.

To examine the development of the microstructure of the material upon heating and cooling, time-resolved temperature-dependent combined SAXS/WAXD measurements were performed on beamline BM26B at the ESFR. Figure 10 shows the different SAXS and WAXD profiles at increasing temperature and clearly reveals the "melting" of the structure.

Above the temperature at which the material starts to flow (140 °C), no structural features were observed in the SAXS pattern, indicating a homogeneous melt state in which the hard blocks are dissolved in the soft phase. In the WAXD pattern, the reflection superimposed on top of the broad amorphous pTHF peak decreases upon heating and eventually disappears completely, demonstrating the melting of the stacks of hydrogen-bonded urea groups.

For SAXS, the total scattering power, Q, which is defined by

$$Q = \int_0^\infty I(s)s^2\,\mathrm{d}s \qquad (2)$$

is plotted as a function of temperature in Figure 11 (left). Both a heating and a cooling run are depicted. The heating curve first shows a gradual decrease of the scattering power. At ∼105 °C, a more rapid decrease was observed, indicating the onset of melting of the ordered structure. For the WAXD, the patterns were deconvoluted into contributions from amorphous and ordered material, and the peak areas of the diffraction corresponding to the stacked urea groups were extracted and plotted as a function of the temperature (Figure 11, right).

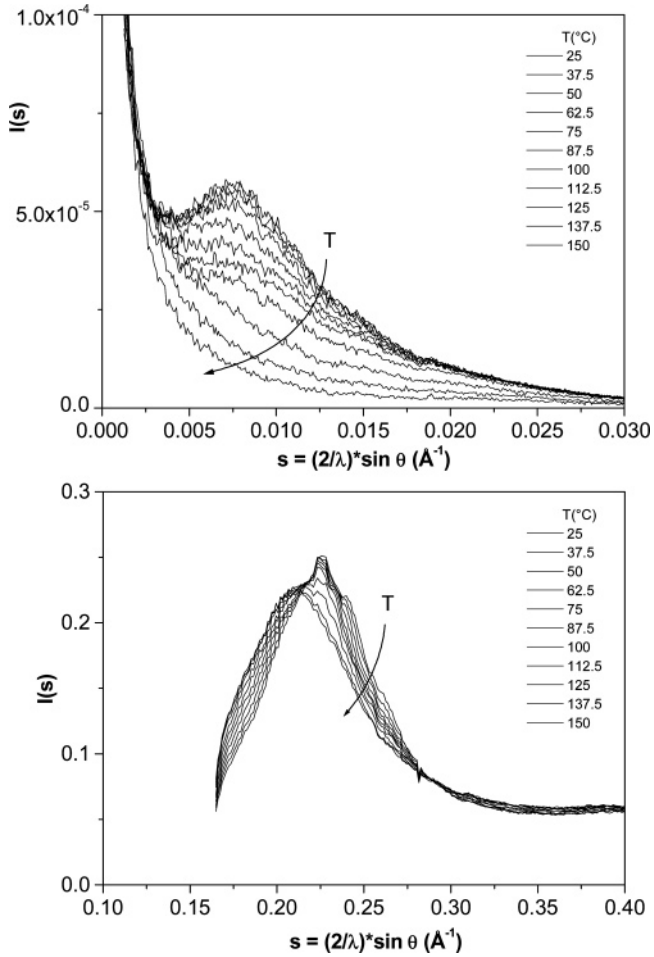

Figure 10. SAXS (top) and WAXD (bottom) profiles during heating of $pTHF_{1100}$-U_2.

The comparison of the evolution of the SAXS and the WAXD intensities reveals a simultaneous decrease of both signals, which suggests the melting and dissolution of the hard domains. The temperature at which this transition occurs is slightly lower than the temperature at which the modulus starts to decrease, as observed by DMTA (120 °C). On the other hand, it corresponds well with the onset of melting that was observed by DSC (ca. 100 °C). Apparently, partial melting of the structure does not immediately result in a decrease of the modulus.

In Figure 11 (left), some hysteresis is observed upon heating and cooling the sample. An undercooling of 15 °C is observed, which is smaller than that observed by DSC (29 °C). This

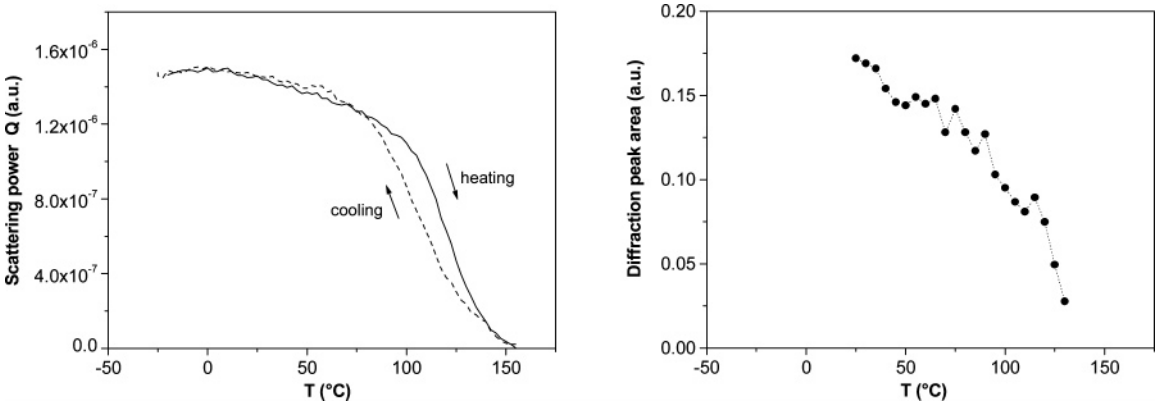

Figure 11. Total scattering power, *Q*, as measured by SAXS (left), and deconvoluted diffraction peak area as measured by WAXD (right), as a function of temperature.

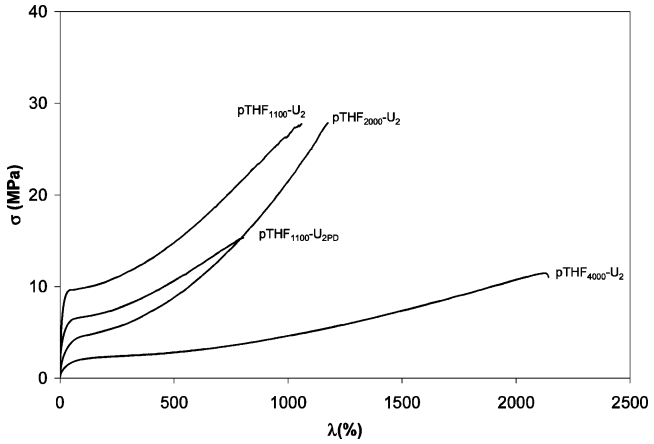

Figure 12. Stress−strain curves for block copoly(ether urea)s.

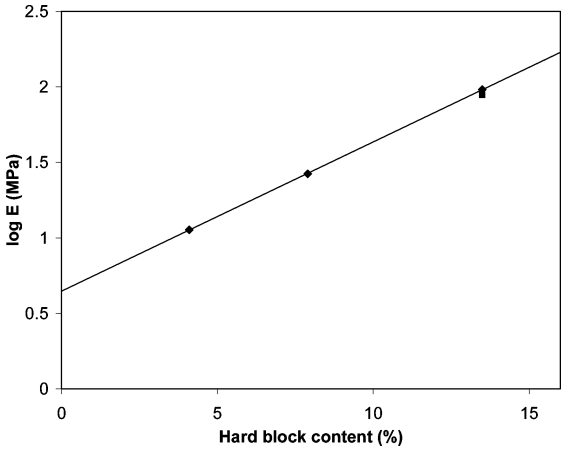

Figure 13. Relation between Young's modulus and hard block content.

Table 4. Tensile Properties of Block Copoly(ether urea)s

copolymer	Young's modulus E (MPa)	strength σ_{br} (MPa)	strain at break λ_{br} (%)	toughness (kJ/kg)
$pTHF_{1100}$-U_2	95.8	27.7	1060	178
$pTHF_{1100}$-U_{2PD}	88.3	15.3	805	80
$pTHF_{2000}$-U_2	25.6	27.8	1175	147
$pTHF_{4000}$-U_2	11.3	11.0	2140	122

discrepancy is partly explained by the different cooling rates employed in both techniques: 5 °C/min for the SAXS and 10 °C/min for DSC. The undercooling is rather small compared to other polymers, like polyethylene, poly(butylene terephthalate), or polyamides,[29] indicating a high rate of crystallization. The temperature at which the reflections representing ordering start to apprear is in the same temperature interval as where the hard segments crystallize. There is no evidence for ordering in the melt prior to crystallization.

3.3. Mechanical Properties. 3.3.1. Tensile Testing. Tensile and elastic properties of the block copoly(ether urea)s with different soft block lengths were studied. Films of these polymers were cast from chloroform/methanol solution, and this procedure yielded completely transparent, flexible films. Tensile bars were punched from these nonoriented films and examined by tensile testing. Figure 12 and Table 4 show the stress−strain behavior of these materials. The strain, λ, is expressed as the ratio between the elongation (ΔL) and the initial length (L_0), in terms of percentage.

The stress−strain curves are typical for thermoplastic elastomeric materials. At small deformations, stress increases linearly with strain (Hookean behavior). The Young's modulus of these polymers increases with decreasing soft block length (increasing hard block content). According to Wegner,[30] the logarithm of the modulus of a segmented copolymer follows a linear relationship with the volume fraction of crystallinity. In our case, when log E is plotted vs the hard block content (see Table 1), the data are confirming this empirical relationship, at least for these four points (Figure 13).

As the stress is increased above a certain value (an indistinct yield point), plastic deformation occurs. At this stage, the stress−strain curve deviates considerably from Hookean behavior, since stress is redistributed by deformation (fragmentation) and reorganization of hard segments. Finally, the polymer cannot bear the load anymore, and the material breaks. The strain at break of these polymers is surprisingly high, ranging from 1000 to 2100%. Harrell[31] and Miller[32] already observed high strains at break for segmented copolyurethanes having a narrow hard segment length distribution. This is caused by the facile deformation and reorganization of thin crystalline lamellae, so the stress is more evenly distributed over the soft segments.[17]

The steep upswing of the stress−strain curve (strain hardening) of $pTHF_{2000}$-U_2 is caused by strain-induced crystallization of the pTHF soft segment. This is evidenced by a whitening of the material. Upon releasing the stress, the soft phase remains semicrystalline, as was proved by DSC. Although $pTHF_{1100}$-U_2 shows a strain hardening effect as well, no strain-induced crystallization is observed, probably since the molecular weight of the soft block is too low to crystallize. Remember, $pTHF_{4000}$ is a random copolymer of THF and ethylene oxide, and this successfully prevents strain-induced crystallization.

The toughness is the energy that is absorbed until the material fails and is reflected by the area under the stress−strain curve. Because of the high strengths and strains at break for these materials, the materials are much tougher than many other

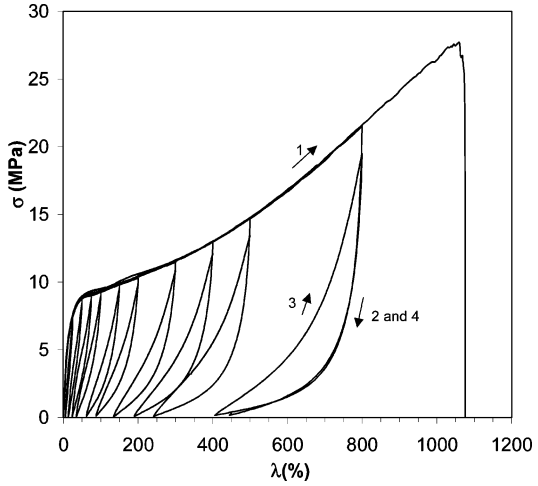

Figure 14. Cyclic tensile test of $pTHF_{1100}$-U_2; testing speed is 100%/min.

thermoplastic elastomers.[1] The toughness of spider dragline silk (~123 kJ/kg)[33] is even exceeded; however, this is not a fair comparison, since spider dragline silk is highly oriented and in this way "predeformed".

The block copoly(ether urea) with the polydisperse hard block, $pTHF_{1100}$-U_{2PD}, possesses inferior properties compared to the analogous one with the uniform hard block, $pTHF_{1100}$-U_2. The Young's modulus, strength, strain at break, and toughness are considerably lower for the former polymer, demonstrating the importance of the well-defined molecular structure for the material properties.

3.3.2. Cyclic Tensile Testing. An important feature of elastomers is the ability to relax to their original dimensions after being deformed. However, complete elastic recovery is rarely observed for thermoplastic elastomers; they usually show some tensile set after being elongated. This is caused by irreversible changes in the morphology of the material during deformation. Once the material has been plastically deformed, the "second" initial modulus is lower compared to the original initial modulus. In general, segmented copolymers with a cocontinuous hard phase show more tensile set than those with a disperse hard phase.[22] Furthermore, strain-induced crystallization increases the tensile set.

The extent of tensile set of the copoly(ether urea)s was determined by performing cyclic tensile tests. The specimen were prestrained to a certain amount of strain, subsequently unloaded and allowed to relax, and again elongated to the same strain (Figure 14). The tensile set is defined as

$$\mathrm{TS} = \frac{L_1 - L_0}{L_0} \times 100\% \qquad (3)$$

in which L_0 is the initial length of the specimen and L_1 is the length after straining and relaxing.

A significant amount of hysteresis is observed for these polymers. In Figure 15 (left), the tensile set is plotted as a function of the prestrain for $pTHF_{1100}$-U_2 and $pTHF_{4000}$-U_2. Per polymer two curves are depicted: one immediately after relaxation and one after 24 h of relaxation. The polymer with the longer soft block, $pTHF_{4000}$-U_2, shows less tensile set than that with the shorter soft block, $pTHF_{1100}$-U_2: a tensile set after 100% prestrain ($TS_{100\%}$) of 6% and 34%, respectively, is observed immediately after deformation. Relaxation of the specimen for 24 h reduces the tensile sets to 4.5% and 25%, respectively. The tensile sets of these materials, especially $pTHF_{1100}$-U_2, are rather high compared to natural rubber ($TS_{100\%}$ < 2%) and segmented copolymers with improved phase separation,[22] but comparable to or lower than those of other thermoplastic elastomeric materials, e.g., block copoly(ether ester)s ($TS_{100\%}$ = 35−40%),[1] block copoly(ether aramid)s ($TS_{300\%}$ = 150−170%),[17] or Spandex ($TS_{100\%}$ = 2−5%).[34] However, the latter comparison is not completely fair, since this value concerns a solution-spun Spandex fiber, which is oriented and in this way "predeformed".

Plastic deformation is also quantified by the hysteresis energy, which is the percentage of energy dissipation within a loading−unloading cycle (difference between areas under the loading and unloading curves).[35,37c] When the hysteresis energy is 0%, all the work (energy) that is put into the sample to deform it is recovered after relaxation (ideal rubber). On the other hand, a hysteresis energy of 100% means that all the work is used to induce irreversible changes in the material, and no work is recovered upon relaxation; the energy is lost as heat. For both polymers, the relative hysteresis energies are plotted in Figure 15 (right). At prestrains above the yield point, almost all energy used to elongate the material is dissipated, resulting in a high amount of tensile set. This is caused by the facile disruption of the hard segments. Once the material has been deformed, the tensile behavior is almost completely reversible (compare traces 2 and 4 in Figure 14). This situation, more or less, resembles the behavior in highly oriented fibers, like solution-spun Spandex fibers.[37c]

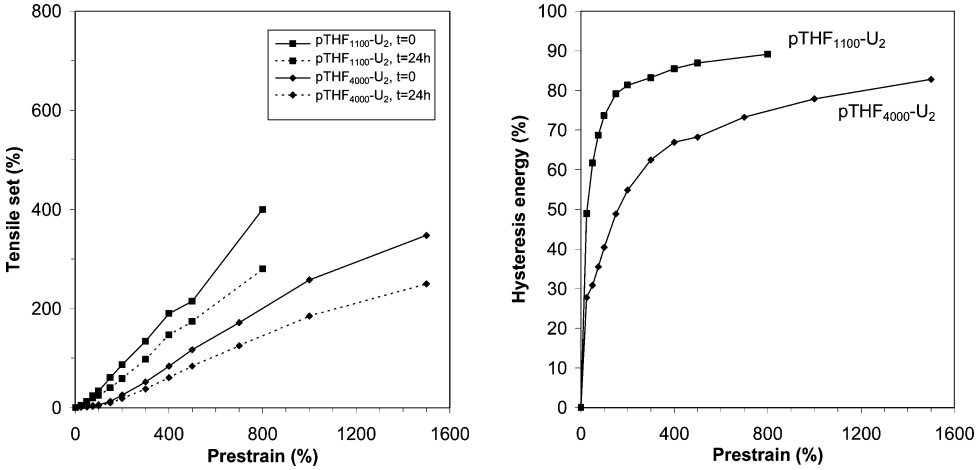

Figure 15. Left: tensile set of two polymers immediately after prestraining and after 24 h. Right: hysteresis energies of these polymers as a function of prestrain.

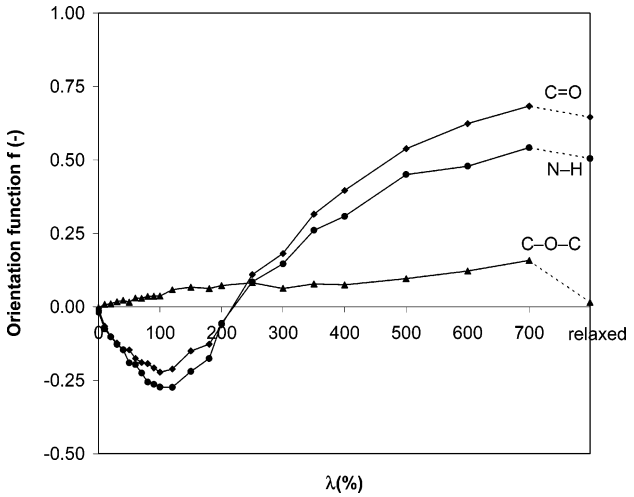

Figure 16. Orientation functions of functional groups in $pTHF_{1100}$-U_2.

3.4. Strain-Induced Orientation of Hard Blocks. In this section, we investigated the changes in morphology and structure during deformation of the block copoly(ether urea)s. Upon elongation (straining) of the native material, orientation and irreversible changes in the morphology of the material occur, resulting in plastic deformation. The orientation in polymers can be measured by several techniques.[36] We decided to use infrared linear dichroism spectroscopy and X-ray scattering techniques to study the structural changes within the material during uniaxial deformation.

3.4.1. Infrared Linear Dichroism. The orientation of functional groups within a polymer is often studied by infrared linear dichroism spectroscopy.[37] In this technique, the absorption of a functional group is measured with polarized infrared light at an angle parallel ($A_{||}$) and perpendicular ($A_{\perp}$) to the stretching direction. The dichroic ratio for such a group is defined as

$$R = A_{||}/A_{\perp} \tag{4}$$

For uniaxial orientation, the degree of orientation is expressed by the Hermans orientation function:

$$f = \frac{(R-1)(R_0+2)}{(R_0-1)(R+2)} = \frac{3\langle\cos^2\beta\rangle - 1}{2} \tag{5}$$

in which β is the angle between the main chain axis and the deformation axis and R_0 is the dichroic ratio for perfect uniaxial orientation and is given by

$$R_0 = 2\cot^2\alpha \tag{6}$$

in which α is the angle between the transition dipole moment of the absorbing group and the main chain axis. The values of α are either described in the literature[37c] or determined from the crystal structure in Figure 2 and are given in Table 5. A distinction is made between peaks arising from the hard and from the soft segments. The first two absorptions are corresponding to the urea groups in the hard segment and the last absorption to the polyether soft segment.

Table 5. Peak Assignments of Selected Infrared Bands of Block Copoly(ether urea)s

peak position (cm^{-1})	assignment	block	α (deg)
3325	N−H stretching	hard	90
1615	C═O stretching	hard	78
1110	C−O−C stretching	soft	0

For randomly oriented groups, $f = 0$; for groups at which the main chain is aligned parallel to the deformation axis, $f = 1$; and for perpendicular alignment, $f = -0.5$. Figure 16 shows the orientation functions of the different functional groups of polymer $pTHF_{1100}$-U_2 with respect to the deformation axis as a function of elongation λ, up to an elongation of 700%. Subsequently, the specimen was released and allowed to relax for several minutes (right side of Figure 16).

As expected, the orientation functions of the three groups are zero before stretching the sample, confirming the nonoriented state of the sample (Figure 17a). The graph shows that at low strain levels, below the yield point, the chain axis in the hard segment is oriented transverse to the deformation axis ($f < 0$). Since the hydrogen-bonded stacks of urea groups are perpendicular to the chain axis, this means that these stacks are oriented parallel to the deformation axis (Figure 17b), which is caused by the high aspect ratio of these hard domains. At these low strains, hardly any orientation of the polyether soft segment is observed.

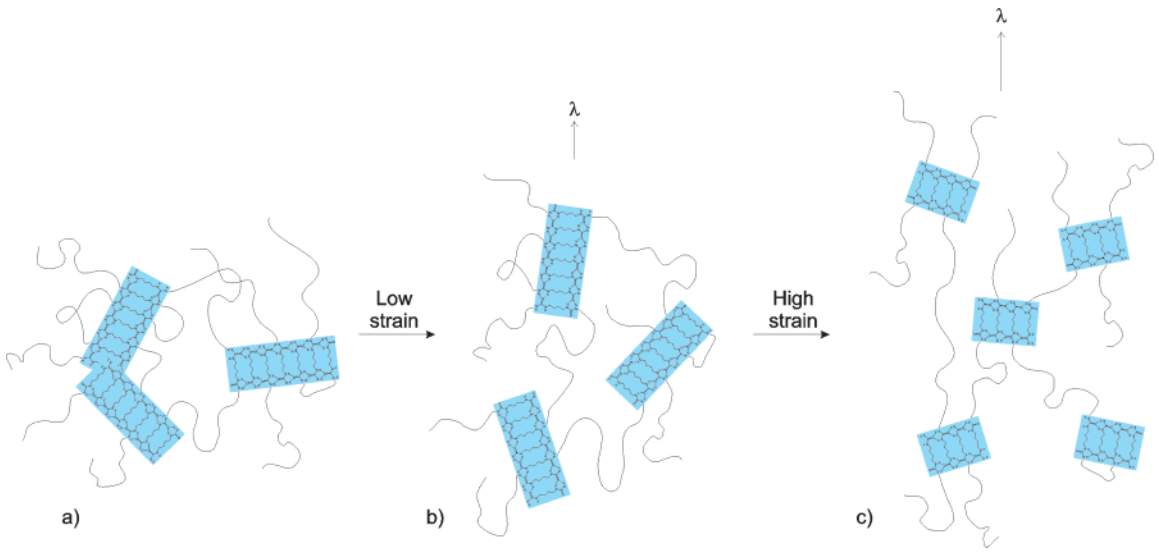

Figure 17. Schematic representation of molecular orientation during tensile testing: (a) nonoriented, (b) below yield point, (c) beyond yield point; not all soft blocks are plotted for clarity.

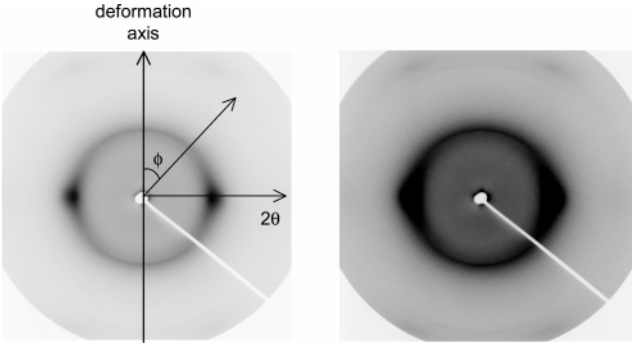

Figure 18. 2D-WAXD patterns of $pTHF_{1100}$-U_2 at 500% strain (left) and after relaxation for 15 min (right).

Above the yield point of the polymer, a different deformation mechanism sets in. Now, the chain axis in the hard segments becomes oriented parallel to the deformation axis ($f > 0$), meaning that the stacks of hydrogen-bonded urea groups (the hard domains) become oriented perpendicular to the deformation axis. To allow this, fragmentation of the hard domains occurs, permitting the reorientation of the hydrogen-bonding stacks (Figure 17c).[35,37] Upon elongation, the polyether soft block is also oriented, as is reflected by the orientation function of ether C−O−C stretching vibration. This indicates orientation of the polymer main chain (and thus the soft segment) in the direction of the deformation.

Releasing the stress on the sample results in relaxation of the soft block to a random coil conformation. No residual orientation of the polyether segment is observed ($f = 0$). In contrast, there is still a high amount of residual orientation of the hard segments, which is responsible for the tensile set of the material. In a second stretch, the orientational behavior is similar to the first stretch.

This orientation behavior upon elongation is comparable to what is described in the literature for other segmented thermoplastic elastomers.[37]

3.4.2. Two-Dimensional Wide-Angle X-ray Diffraction. X-ray scattering techniques, both WAXD and SAXS, are very suitable to study orientation of polymeric materials.[23f,27a,f,36,38] Especially, a combination of these techniques with microscopic techniques (e.g., AFM) is very powerful.[39]

The orientation of polymer $pTHF_{1100}$-U_2 during tensile testing was studied by time-resolved 2D-WAXD measurements. A typical result obtained at a strain of 500% is shown in Figure 18 (left). Only two reflections (each other's mirror image) are visible on the equator at a *d* spacing of ∼4.5 Å. Because of the low crystallinity of the material, and the overlap of the reflection corresponding to the hard block with the amorphous pTHF halo (see Figure 7), no conclusions can be drawn concerning the orientation of the distinct segments in this polymer upon elongation. Nevertheless, since these reflections are observed on the equator, perpendicular to the deformation axis, the overall orientation within the elongated specimen should be perpendicular to the deformation axis as well (Figure 17c). Strain-induced crystallization is not detected, since no reflection corresponding to a crystalline pTHF phase are observed.[25] Relaxation of the applied stress results in partial recovery of the amorphous halo (Figure 18, right). Some remaining orientation is observed, as the reflections on the equator are still visible.

3.4.3. Two-Dimensional Small-Angle X-ray Diffraction. The orientation and reorganization of the different segments in block copoly(ether urea) $pTHF_{1100}$-U_2 were studied using 2D-SAXS measurements. Because of the absence of a tensile tester suitable for these measurements, the samples were prestrained to a specific deformation, allowed to relax for 2 days, and subsequently measured.

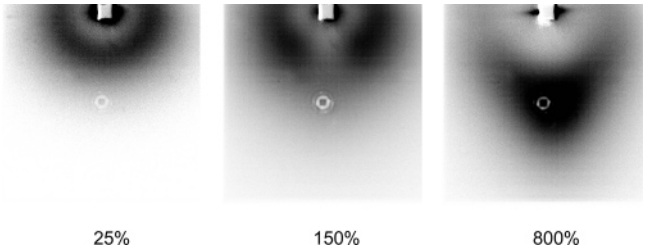

Figure 19. 2D-SAXS patterns recorded from $pTHF_{1100}$-U_2 after prestraining to specified deformation; deformation axis is vertical.

Figure 19 shows three SAXS patterns (only the lower half) at different amounts of prestrain. The circular spot in the middle of the patterns is a defect due to damaging of the detector. The pattern at 25% prestrain reveals a nonoriented morphology due to full reversibility of the microstructure. At 150% prestrain a four-spot pattern and at 800% prestrain a two-spot pattern are observed.

The four-spot pattern develops upon deformations higher than 100% and is observed up to deformations of 500%. It indicates that there are correlations among the hard domains not only parallel but also perpendicular to the deformation axis. We attribute this four-spot pattern to the tilted formation of the hard blocks along the deformation axis (Figure 17b). This type of orientation of hard blocks in segmented copolymers has been reported before by Bonart[24] and Hsiao[40] and is caused by the high aspect ratio of these domains.

The two-spot pattern is superimposed on the four-spot pattern after deformations higher than 500%, and it dominates the scattering pattern above 800%. It indicates the presence of rather small, fragmented, crystalline domains that are ordered in stacks with correlations among the stacks only in the direction parallel to the deformation axis and not in the lateral direction (Figure 17c). Further analysis of this two-spot pattern, by plotting the intensities recorded perpendicular to the deformation axis in a Guinier plot,[41] revealed an average dimension of the hard domains after deformation of ∼5 nm. This is significantly smaller than the length of the hard domains as found by AFM (Figure 6), which reached over 500 nm. This decrease is due to the fragmentation of the hard domains at high deformation values.

It would be highly interesting to study the fragmentation of the hard domains upon elongation in real-time by X-ray scattering techniques. However, attempts to do so were unsuccessful so far, due to the low crystallinity of the material and the limited thickness of the tensile bars that were used for this purpose.

4. Conclusions

The detailed study presented above demonstrates that block copoly(ether urea)s with exactly two urea groups in the hard blocks, $pTHF_y$-U_2, are thermoplastic elastomers with mechanical properties superior to a less-defined analogue possessing polydisperse hard blocks. The mechanical properties are also equal to or even surpass those of many other thermoplastic elastomers. The strain at break (1000−2100%) and toughness of these materials are higher than for commercially available TPEs, e.g., block copolyesters (trade name Hytrel or Arnitel), block copolyamides (Pebax, Vestamid), or block copolyurethanes (Desmopan, Elastane). Another advantage of $pTHF_y$-U_2 block copoly(ether urea)s is that, in contrast to many other TPEs, they are completely transparent. We have demonstrated that the

unique properties of these polymers are the result of strong hydrogen bonding between the urea groups within the hard blocks. These strong and directional interactions result in the formation of very thin hard blocks. The hard blocks are also very uniform, resulting in a morphology resembling that of a nanocomposite. The absence of phase mixing between hard and soft phases at room temperature results in a low glass transition temperature and an extended, temperature-independent rubbery plateau with good low-temperature flexibility. Around the melting point of the hard blocks of the polymer (ranging from 100 to 165 °C), the material becomes liquidlike and begins to flow. Because the melting point is well below the decomposition temperature of the polymer, melting is completely reversible, and the polymers may potentially be melt-spun to produce highly oriented, elastic fibers. This procedure would be advantageous with respect to the more expensive solution spinning that is currently used for the fabrication of Spandex fibers.[37c]

The study of molecular orientation of $pTHF_y$-U_2 block copoly(ether urea)s upon deformation of the material shows that two reorientation processes occur. Below the yield point, the hard domains tilt in a direction parallel to the deformation axis due to their high aspect ratio. In contrast, above the yield point, fragmentation and reorientation of the hard domains occur, resulting in a perpendicular orientation. Upon releasing the stretched material, the soft segment relaxes to the nonoriented state, but the hard domains remain oriented. While this leads to a considerable amount of tensile set, the mechanically induced orientation of the hard blocks also offers unique opportunities to tune optical properties of guest molecules, which—as was recently shown by us[15]—may be selectively incorporated in the hard blocks through the strong and well-defined urea−urea hydrogen-bonding motif.

Acknowledgment. We acknowledge H. Kooijman, A. L. Spek, R. G. H. Lammertink, J. G. P. Goossens, L. E. Govaert, and O. L. J. van Asselen for their experimental help and analyses. Support from the Council for Chemical Sciences of the Netherlands Organization for Scientific Research (CW-NWO) with financial aid from the Netherlands Technology Foundation (STW) is gratefully acknowledged.

References and Notes

(1) Legge, N. R.; Holden, G.; Schroeder, H. E. *Thermoplastic Elastomers: A Comprehensive Review*; Carl Hansser Verslag: New York, 1987.
(2) Mark, H. F. *Encyclopedia of Polymer Science and Technology*, 3rd ed.; Wiley-Interscience: New York, 2001.
(3) (a) Kennedy, J. P.; Castner, K. F. *J. Polym. Sci., Part A* **1979**, *17*, 2055. (b) Engle, L. P.; Wagener, K. B. *J. Macromol. Sci., Rev.* **1993**, *C33*, 239.
(4) (a) Hilger, S.; Stadler, R. *Macromolecules* **1992**, *25*, 6670. (b) Abetz, V.; Dardin, A.; Stadler, R.; Hellman, J.; Samulski, E. T.; Spiess, H.-W. *Colloid Polym. Sci.* **1996**, *274*, 723.
(5) Ullmann, F. *Ullmann's Encyclopedia of Industrial Chemistry*, 6th ed.; VCH: Weinheim, 2001.
(6) (a) Coleman, D. *J. Polym. Sci.* **1954**, *14*, 15. (b) Witsiepe, W. K. *ACS Adv. Chem.* **1973**, *129*, 39.
(7) Deleens, G.; Foy, P.; Marechal, E. *Eur. Polym. J.* **1977**, *13*, 337.
(8) Bayer, O.; Muller, E.; Petersen, S.; Piepenbrink, H. F.; Windemuth, E. *Angew. Chem.* **1950**, *62*, 57.
(9) Cella, R. J. *J. Polym. Sci., Symp.* **1973**, *42*, 727.
(10) Sorta, E.; Melis, A. *Polymer* **1978**, *19*, 1153.
(11) (a) Harrell, L. L. *Macromolecules* **1969**, *2*, 607. (b) Ng, H. N.; Allegrezza, A. E.; Seymour, R. W.; Cooper, S. L. *Polymer* **1973**, *14*, 255. (c) Eisenbach, C. D.; Baumgartner, M.; Gunter, G. *Adv. Elastomers Rubber Elasticity [Proc. Symp.]* **1985**, *51*. (d) Miller, J. A.; Shaow, B. L.; Hwang, K. K. S.; Wu, K. S.; Gibson, P. E.; Cooper, S. L. *Macromolecules* **1985**, *18*, 32. (e) Shirasaka, H.; Inoue, S.-i.; Asai, K.; Okamoto, H. *Macromolecules* **2000**, *33*, 2776. (f) Lai, Y.-C.; Quinn, E. T.; Valint, P. L., Jr. *J. Polym. Sci., Part A* **1995**, *33*, 1767. (g) Blundell, D. J.; Eeckhaut, G.; Fuller, W.; Mahendrasingam, A.; Martin, C. *Polymer* **2002**, *43*, 5197. (h) Christianson, C. P.; Harthcock, M. A.; Meadows, M. D.; Spell, H. L.; Howard, W. L.; Creswick, H. W.; Guerra, R. E.; Turner, R. B. *J. Polym. Sci., Part B* **1986**, *24*, 1401. (i) Samuels, S. L.; Wilkes, G. L. *J. Polym. Sci., Symp.* **1973**, *43*, 149.
(12) (a) Gaymans, R. J.; Haan, J. L. d. *Polymer* **1993**, *34*, 4360. (b) Niesten, M. C. E. J.; Gaymans, R. J.; Brinke, A. t. *Polym. Prepr.* **1999**, *40*, 1012. (c) Niesten, M. C. E. J.; Gaymans, R. J.; Brinke, A. t. *Polym. Prepr.* **1999**, *40*, 1012. (d) Niesten, M. C. E. J.; Harkema, S.; van der Heide, E.; Gaymans, R. J. *Polymer* **2000**, *42*, 1131. (e) Niesten, M. C. E. J.; Tol, R.; Gaymans, R. J. *Polymer* **2000**, *42*, 931. (f) Niesten, M. C. E. J.; Feijen, J.; Gaymans, R. J. *Polymer* **2000**, *41*, 8487. (g) Niesten, M. C. E. J.; Gaymans, R. J. *J. Appl. Polym. Sci.* **2001**, *81*, 1372. (i) Niesten, M. C. E. J.; Gaymans, R. J. *Polymer* **2001**, *42*, 6199.
(13) (a) Yilgor, I.; Sha'aban, A. K.; Steckle, W. P., Jr.; Tyagi, D.; Wilkes, G. L.; McGrath, J. E. *Polymer* **1984**, *25*, 1800. (b) Tyagi, D.; Yilgor, I.; McGrath, J. E.; Wilkes, G. L. *Polymer* **1984**, *25*, 1807. (c) Marcos-Fernandez, A.; Lozano, A. E.; Gonzalez, L.; Rodriguez, A. *Macromolecules* **1997**, *30*, 3584. (d) Yilgor, E.; Burgaz, E.; Yurtsever, E.; Yilgor, I. *Polymer* **1999**, *41*, 849. (e) Yilgor, E.; Yilgor, I. *Polymer* **2001**, *42*, 7953. (f) Riess, G.; Mendolia, M. S.; Schmidt, H.-W. *Macromol. Symp.* **2002**, *181*, 123. (g) Yilgor, I.; Mather, B. D.; Unal, S.; Yilgor, E.; Long, T. E. *Polymer* **2004**, *45*, 5829. (h) Sheth, J. P.; Aneja, A.; Wilkes, G. L.; Yilgor, E.; Atilla, G. E.; Yilgor, I.; Beyer, F. L. *Polymer* **2004**, *45*, 6919. (i) Colombani, O.; Barioz, C.; Bouteiller, L.; Chaneac, C.; Fomperie, L.; Lortie, F.; Montes, H. *Macromolecules* **2005**, *38*, 1752. (j) Sheth, J. P.; Klinedinst, D. B.; Wilkes, G. L.; Yilgor, I.; Yilgor, E. *Polymer* **2005**, *46*, 7317.
(14) Versteegen, R. M.; Sijbesma, R. P.; Meijer, E. W. *Macromolecules* **2005**, *38*, 3176.
(15) Koevoets, R. A.; Versteegen, R. M.; Kooijman, H.; Spek, A. L.; Sijbesma, R. P.; Meijer, E. W. *J. Am. Chem. Soc.* **2005**, *127*, 2999.
(16) (a) Born, L.; Hespe, H. *Colloid Polym. Sci.* **1985**, *263*, 335. (b) van Esch, J.; De Feyter, S.; Kellogg, R. M.; De Schryver, F.; Feringa, B. L. *Chem.—Eur. J.* **1997**, *3*, 1238. (c) Van Esch, J.; Schoonbeek, F.; De Loos, M.; Kooijman, H.; Spek, A. L.; Kellogg, R. M.; Feringa, B. L. *Chem.—Eur. J.* **1999**, *5*, 937. (d) De Loos, M.; Ligtenbarg, A. G. J.; Van Esch, J.; Kooijman, H.; Spek, A. L.; Hage, R.; Kellogg, R. M.; Feringa, B. L. *Eur. J. Org. Chem.* **2000**, 3675. (e) Gesquiere, A.; Abdel-Mottaleb, M. M. S.; De Feyter, S.; De Schryver, F. C.; Schoonbeek, F.; van Esch, J.; Kellogg, R. M.; Feringa, B. L.; Calderone, A.; Lazzaroni, R.; Bredas, J. L. *Langmuir* **2000**, *16*, 10385. (f) Etter, M. C.; Urbanczyk-Lipkowska, Z.; Zia-Ebrahimi, M.; Panunto, T. W. *J. Am. Chem. Soc.* **1990**, *112*, 8415. (g) Carr, A. J.; Melendez, R.; Geib, S. J.; Hamilton, A. D. *Tetrahedron Lett.* **1998**, *39*, 7447. (h) Pathirana, H. M. K. K.; Weiss, T. J.; Reibenspies, J. H.; Zingaro, R. A.; Meyers, E. A. *Z. Kristallogr.* **1994**, *209*, 696. (i) Perez-Folch, J.; Subirana, J. A.; Aymami, J. *J. Chem. Crystallogr.* **1997**, *27*, 367.
(17) Niesten, M. Ph.D. Thesis, University of Twente (Enschede), 2000.
(18) Olabisi, O. *Polyester-Based Thermoplastic Elastomers*; Marcel Dekker: New York, 1997; p 1053.
(19) Mark, H. F.; Bikales, N. M.; Overberger, C. G.; Mengers, G. *Encyclopedia of Polymer Science and Engineering*, 2nd ed.; Wiley-Interscience: New York, 1985.
(20) Coleman, M. M.; Sobkowiak, M.; Pehlert, G. J.; Painter, P. C.; Iqbal, T. *Macromol. Chem. Phys.* **1997**, *198*, 117.
(21) Saunders, J. H.; Frisch, K. C. *Polyurethanes: Chemistry and Technology, Part 1 Chemistry*; Interscience: New York, 1962; Vol. 16.
(22) Schmalz, H.; van Guldener, V.; Gabrieelse, W.; Lange, R.; Abetz, V. *Macromolecules* **2002**, *35*, 5491.
(23) (a) Garrett, J. T.; Lin, J. S.; Runt, J. *Macromolecules* **2002**, *35*, 161. (b) Garrett, J. T.; Runt, J.; Lin, J. S. *Macromolecules* **2000**, *33*, 6353. (c) Savelyev, Y. V.; Akhranovich, E. R.; Grekov, A. P.; Privalko, E. G.; Korskanov, V. V.; Shtompel, V. I.; Privalko, V. P.; Pissis, P.; Kanapitsas, A. *Polymer* **1998**, *39*, 3425. (d) Musselman, S. G.; Santosusso, T. M.; Barnes, J. D.; Sperling, L. H. *J. Polym. Sci.* **1999**, *37*, 2586. (e) Veenstra, H.; Hoogvliet, R. M.; Norder, B.; De Boer, A. P. *J. Polym. Sci., Part B* **1998**, *36*, 1795. (f) Chu, B.; Hsiao, B. S. *Chem. Rev.* **2001**, *101*, 1727.
(24) (a) Bonart, R. *J. Macromol. Sci., Part B* **1968**, *2*, 115. (b) Bonart, R.; Müller, E. H. *J. Macromol. Sci., Phys.* **1974**, *B10*, 177. (c) Bonart, R.; Müller, E. H. *J. Macromol. Sci., Phys.* **1974**, *B10*, 345.
(25) Cesari, M.; Perego, G.; Mazzei, A. *Makromol. Chem.* **1965**, *83*, 196.
(26) Strobl, G. R.; Schneider, M. *J. Polym. Sci., Part B* **1980**, *18*, 1343.
(27) Goderis, B.; Reynaers, H.; Koch, M. H. J. *Macromolecules* **2002**, *35*, 5840.
(28) (a) Phillips, R. A.; Cooper, S. L. *Macromolecules* **1995**, *28*, 5734. (b) Velankar, S.; Cooper, S. L. *Macromolecules* **2000**, *33*, 382. (c) Heck, B.; Arends, P.; Ganter, M.; Kressler, J.; Stuehn, B. *Macromolecules* **1997**, *30*, 4559.
(29) (a) Koutsky, J. A.; Walton, A. G.; Baer, E. *J. Appl. Phys.* **1967**, *38*, 1832. (b) van Bennekom, A. C. M.; Gaymans, R. J. *Polymer* **1997**, *38*, 657.

(30) Wegner, G. In Legge, N. R., Holden, G., Schroeder, H. E., Eds.; *Thermoplastic Elastomers: A Comprehensive Review*; Carl Hansser Verslag: New York, 1987; Section 12/5.

(31) Harrell, L. L. *Macromolecules* **1969**, *2*, 607.

(32) Miller, J. A.; Shaow, B. L.; Hwang, K. K. S.; Wu, K. S.; Gibson, P. E.; Cooper, S. L. *Macromolecules* **1985**, *18*, 32.

(33) Kubik, S. *Angew. Chem., Int. Ed.* **2002**, *41*, 2721.

(34) Ullmann, F. *Ullmann's Encyclopedia of Industrial Chemistry*, 6th ed.; VCH: Weinheim, 2001.

(35) Wang, C. B.; Cooper, S. L. *Macromolecules* **1983**, *16*, 775.

(36) Ward, I. M. *Structure and Properties of Oriented Polymers*, 2nd ed.; Chapman & Hall: London, 1997.

(37) (a) Van der Heide, E.; Van Asselen, O. L. J.; Ingenbleek, G. W. H.; Putman, C. A. J. *Macromol. Symp.* **1999**, *147*, 127. (b) Lee, H. S.; Hsu, S. L. *J. Polym. Sci., Part B* **1994**, *32*, 2085. (c) Lee, H. S.; Ko, J. H.; Song, K. S.; Choi, K. H. *J. Polym. Sci., Part B* **1997**, *35*, 1821. (d) Kischel, M.; Kisters, D.; Strohe, G.; Veeman, W. S. *Eur. Polym. J.* **1998**, *34*, 1571. (e) Graff, D. K.; Wang, H.; Palmer, R. A.; Schoonover, J. R. *Macromolecules* **1999**, *32*, 7147. (f) Lee, H. S.; Ko, J. H.; Song, K. S.; Choi, K. H. *J. Polym. Sci., Part B* **1997**, *35*, 1821.

(38) Blundell, D. J.; Eeckhaut, G.; Fuller, W.; Mahendrasingam, A.; Martin, C. *Polymer* **2002**, *43*, 5197.

(39) Sauer, B. B.; McLean, R. S.; Brill, D. J.; Londono, D. J. *J. Polym. Sci., Part B* **2002**, *40*, 1727.

(40) Yeh, F.; Hsiao, B. S.; Sauer, B. *Polym. Mater. Sci. Eng.* **1998**, *79*, 332.

(41) (a) Schultz, J. M.; Lin, J. S.; Hendricks, R. W. *J. Appl. Crystallogr.* **1978**, *11*, 551. (b) Tan, S.; Zhang, D.; Zhou, E. *Polym. Int.* **1997**, *42*, 90.

MA051874E